Relaxation effect on crystal nucleation in a glass unveiled by experimental, numerical, and analytical approaches

Lorena R. Rodrigues [a], Alexander S. Abyzov [b,a], Vladimir M. Fokin [c,a], Jürn W. P. Schmelzer[d], Edgar D. Zanotto [a]

[a]Department of Materials Engineering, Center for Research, Technology and Education in Vitreous Materials, Federal University of São Carlos, São Carlos, Brazil

[b]National Science Center Kharkov Institute of Physics and Technology, Kharkov, Ukraine

[c]Department of Chemical Engineering, Federal University of Bahia, Brazil

[d]Institut für Physik der Universität Rostock, Albert-Einstein-Strasse 23-25, 18059 Rostock, Germany

Abstract

Understanding the mechanisms and dynamics of crystal nucleation and growth in glass-forming materials is fundamental to avoid or control crystallization - the critical steps for developing and producing novel glasses and glass-ceramics. Below the temperature T_{max}, corresponding to the maximum of experimentally measured nucleation rates, the reported nucleation rates are frequently smaller than the theoretical predictions by the Classical Nucleation Theory (CNT). This discrepancy dramatically increases with decreasing temperature, and has been denoted as the "breakdown" of the CNT. For understanding this alleged breakdown, it is important to stress that the experimental T_{max} is located somewhat above or at the glass transition temperature, T_g. Here, using a 5BaO·8SiO2 (B_5S_8) glass, first, we showed a significant change in the characteristic relaxation time with temperature in the T_g region: it is four times shorter for the supercooled liquid than for the glass. Then a combination of detailed experiments and theoretical (analytical and numerical) analyses for the B_5S_8 glass confirmed our recent findings for $Li_2O{\cdot}2SiO_2$ and $2Na_2O{\cdot}CaO{\cdot}3SiO_2$ glasses. The "breakdown" is just an artefact, since the experimental nucleation times used are often not long enough to allow the complete structural relaxation of the glass and hence reach the ultimate steady-state nucleation rate. Finally, for the first time, we also show that due to the almost complete crystallization of the B_5S_8 glass, and likely of other glasses that exhibit sufficiently high nucleation and growth rates, the structural relaxation process cannot be finished and, correspondingly, the ultimate steady-state nucleation regime at $T < T_{max}$ *cannot* be reached. This new finding further explains the failure of several previous works to reach the definitive, ultimate steady-state nucleation regime at low temperatures.

Keywords: Glass, nucleation, crystal growth, crystallization, relaxation, glass transition, phase transition

1 Introduction

The correct understanding of crystal nucleation and growth processes in glass-forming materials is of fundamental importance to avoid or control crystallization, which are preconditions for the development and production of glasses and glass-ceramics. Crystallization kinetics is frequently analyzed in the framework of the Classical Nucleation Theory (CNT). At relatively high temperatures, above the laboratory glass transition, T_g, the CNT allows a quantitative description of the temperature dependence of nucleation rates. Experiments show that the temperature T_{max}, corresponding to the maximum of the experimentally measured nucleation rates in oxide glass-formers, occurs in the glass transition range, $T_{max} \approx T_g$. However, at low temperatures, below T_{max}, the reported nucleation rates are typically smaller than the theoretically predicted values. This discrepancy between experimental data and theoretical predictions dramatically increases with decreasing temperature, and has been denoted as the "breakdown" of the CNT. The low-temperature nucleation rate anomaly is also observed in non-classical nucleation theories, including the self-consistent classical theory [1,2] and different versions of the density functional theory [3]. However, as demonstrated in preceding papers [4-6], this notation is inappropriate. In these papers, we reanalyzed nucleation experiments in the low temperature range $T \leq T_{max}$, and showed that the CNT is indeed able to adequately describe nucleation kinetics if *relaxation* effects are properly accounted for. Such effects are negligible at higher temperatures above the glass transition temperature, T_g, but can be very significant at low temperatures.

The origin of this discrepancy between experiment and the CNT and its resolution is the following: experimental crystal nucleation data are usually determined in restricted laboratory time scales. As the maxima of the steady-state nucleation rates found in commonly used experimental procedures are located close to T_g, which corresponds to a high liquid viscosity, of the order of ~10^{12} Pa·s, the characteristic relaxation times start to become very long below this temperature. Therefore, the evolution of the glass structure to that of the corresponding equilibrium supercooled liquid requires a considerable time in this temperature range, $T \leq T_{max}$. Consequently, we must incorporate deviations of the glass structure from equilibrium into the CNT. In addition, because the glass structure changes with time due to relaxation, the crystallization kinetics also varies until the metastable state of the liquid is eventually reached. However, at $T \ll T_{max}$, this final state may not be reached at all within the restricted experimental time scales typically used due to complete crystallization of the residual glass prior to full relaxation. We will demonstrate this problem, for the first time, in the Discussion section.

As a first example of taking relaxation into account during nucleation, we recently performed an in-depth analysis of experimental nucleation data in a lithium disilicate glass

($Li_2O{\cdot}2SiO_2$) at $T < T_{max}$ using newly derived analytical expressions within the CNT framework. This analysis demonstrated a strong effect of structural relaxation on the nucleation kinetics [4,5]. We have shown in these articles that the time evolution (increase) of the nucleation rate at low temperatures, previously interpreted by several authors (including ourselves) as being a sign of the classical concept of non-stationary nucleation rate, mainly results from structural relaxation. Thus, the often-reported discrepancy between experiment and theory below the experimental T_{max} is due to the fact that, at these low temperatures below T_g, the experimental nucleation times normally used are not sufficiently long to complete the structural relaxation of the glass, and thus to reach the ultimate steady-state nucleation regime. Hence, the measured nucleation rates are frequently smaller than the ultimate values. Such deviations of the glass and intermediate liquid from equilibrium have not been accounted for earlier in the description of nucleation rates, except in our previous papers on $Li_2O{\cdot}2SiO_2$ glass [4,5]. Taking them appropriately into account, the CNT adequately describes nucleation rates from the beginning of crystallization process up to the final stage, when relaxation is completed. This effect of structural relaxation on the nucleation kinetics was also recently demonstrated for a soda-lime-silica ($2Na_2O{\cdot}CaO{\cdot}3SiO_2$) glass [6], where we showed that the actual T_{tmax} is located well below the typically reported experimental T_{max}.

In the present work, we expand and generalize the experimental basis for further development of this new approach to interpret nucleation kinetics in glasses and deeply supercooled glass-forming liquids. For these purposes, we used a scarcely studied barium silicate glass ($5BaO{\cdot}8SiO_2$) that reveals homogeneous volume nucleation when properly heated [7-10]. We obtained new nucleation data and, for the first time, they were analyzed by combining numerical simulations for the very beginning of the nucleation process with analytical expressions for its advanced stages. Also, further interesting new findings concerning particular features of crystallization of deeply supercooled liquids were discovered, and will be reported in the following sections.

2 Materials and Methods

For our experiments, a 250 g batch of B_5S_8 glass was prepared by mixing SiO_2 (Zetasil 4, ≥99.99%) and $BaCO_3$ (Alfa Aesar, 99.8%) at specific ratios in a TURBULA T10B mixer for 4 h. The chemicals were calcined in a Pt crucible at 1653 K for 48 h using an electrical furnace, and then melted at 1823 K for ~30 min. In addition to decomposing $BaCO_3$, the calcination treatment promoted formation of the $Ba_5Si_8O_{21}$ phase, which aided the glass chemical homogeneity. To further improve the chemical homogeneity, the glass was crushed and re-melted twice. Thereafter, the melt was splat-cooled between two steel plates, forming 2-3 mm-thick glass samples. To avoid

incipient nucleation, no annealing treatment was performed. We confirmed the high chemical homogeneity degree of this glass batch by a rigorous statistical method [11]. The glass transition temperature (DSC-T_g) was determined through differential scanning calorimetry (Netzsch DSC 404) with a Pt pan and lid, using small monolithic pieces, at a heating rate of 10 K/min.

Isothermal heat treatments at $T = 1093, 1103, 1118, 1133$ and $1143\ K$ were performed to measure the crystal growth velocity $U(T) = dR_M/dt$, where R_M is the radius of the largest crystal in micrographs of the sample cross-section. As shown in Fig. 1, the B_5S_8 crystals are spherical.

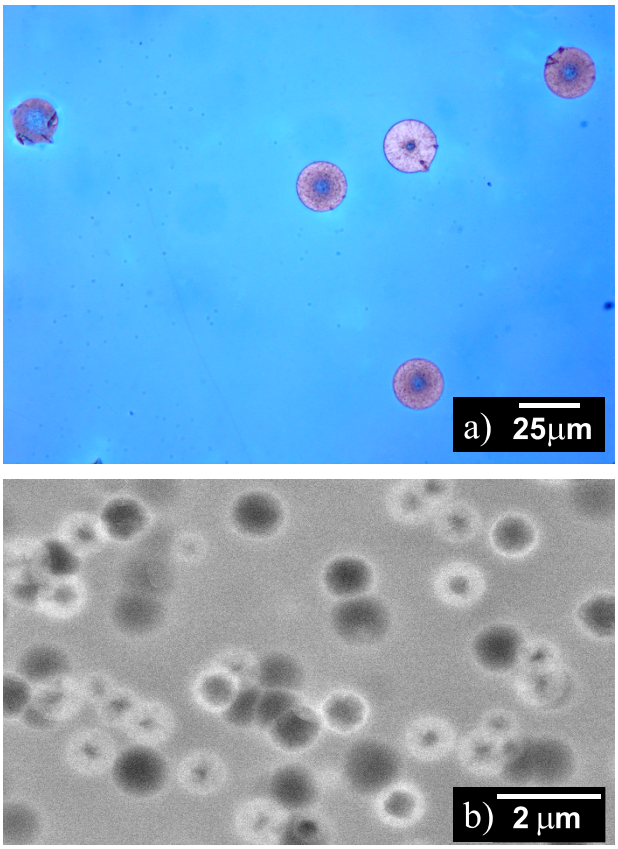

Fig. 1. Reflected light optical micrograph of a B_5S_8 sample cross-section treated at 1133 K for 6 min (a); SEM micrograph of a B_5S_8 sample cross-section treated at 958 K for 32.5 h and then at 1085 K for 3 min (b).

To estimate the time dependence of the crystal number density, $N_v(t)$, we used the Tammann's method of double-stage heat treatment. The samples were first subjected to a given nucleation temperature, T_n, for different times and then to a development treatment at a temperature T_d to grow the crystal nuclei to detectable sizes. The T_d temperatures were chosen to satisfy the following conditions for the rates of nucleation, I, and growth, U: $I(T_d) \ll I(T_n)$ and $U($

$T_d) \gg U(T_n)$. The nucleation treatments were carried out at different temperatures in the 948-1053 K range, which were followed by development at 1085 K ($T_n = 948...983$ K) or 1103 K ($T_n = 978...1053$ K).

Heat treatments for crystal nucleation and growth were performed in vertical electrical furnaces at given temperatures measured with a precision of ±2 K using calibrated thermocouples. After the nucleation and growth heat treatments, the samples were sequentially ground using 320-1200 grit SiC papers, polished with a CeO_2 suspension, and etched with a 2 vol% HF solution for ~10 s to reveal the crystals on the cross-sections. Then they were observed by reflected light optical microscopy (Leica DMRX and Nikon Eclipse LV100N POL). Samples heat treated at $T_n = 948$ K for $t_n \geq 65$ h and at 958 K for $t_n \geq 32.5$ h were analyzed by Scanning Electron Microscopy (SEM) (Philips XL-30 FEG), Fig.1b.

For spherical crystals of the same size (approximately our case), the crystal number density is related to the number of crystals, N_s, per unit area of sample cross-section via Eq. (1) [12]

$$N_v = \frac{N_s}{2R}\,, \tag{1}$$

where R is the crystal radius, which is equal to the radius of largest crystal in the cross-section.

It should be noted that the development of nucleated crystals in the Tammann's method leads to an almost mono-disperse crystal size distribution [12] if the crystal growth velocities are very small at the different T_n. In our case, the size distribution width after development does not exceed 0.1 micron, and it can be neglected in comparison with the typical average size, which in our experiments was ≥1-2 micron.

However, due to the resolution limit, ε, of optical microscopes, the number of crystals, N_s, in the sample cross-section may be underestimated, i.e., some crystal cuts are below ε. The underestimated fraction of N_s can be evaluated by Eq. (2), derived in [13],

$$f = \frac{2}{\pi}\sin^{-1}\frac{\varepsilon}{D_M}, \tag{2}$$

where: ε is the resolution limit of the microscope (in our case ε is in the range $0.3...0.7$ μm, depending on the microscope objective used) and $D_M = 2R_M$ is the size of the largest crystal in the sample cross-section. Thus, the corrected crystal number density, N, is given by Eq.(3)

$$N = \frac{N_v}{1-f}\,. \tag{3}$$

3 Basic Equations

We analyzed the nucleation rates within the framework of the CNT using both numerical simulations and analytical methods. In both cases, we considered the effect of structural relaxation of the supercooled liquid (SCL) on the main parameters determining the nucleation process. For this analysis, we introduced the factor $\zeta(t)$, which correlates with the structural order parameter, ξ, as in [4,6]

$$\zeta = 1 + \left(\frac{\xi - \xi_{eq}}{\xi_{eq}}\right)^2. \tag{4}$$

Thereafter, the subscript *eq* indicates that the value refers to a fully relaxed equilibrium SCL (the detailed theory is given in [5]).

In [4,6], we showed that, for lithium silicate and sodium calcium silicate glasses, the nucleation time-lag, τ_{CK}, characterizing the establishment of the classical stationary regime of the nucleation process is much shorter than the characteristic structural relaxation time. Similar results were obtained here for the $5BaO{\cdot}8SiO_2$ glass (Table 1). Thus, at every moment of time, the nucleation rate is close to its current steady-state value, I_{st}, corresponding to the current state of the relaxing glass structure. However, only after the relaxation process is completed, i.e., the SCL equilibrium state is reached, the ultimate steady-state nucleation regime is established.

The following equation for the steady-state nucleation rate, I_{st}, in *a relaxing* glass or SCL, was obtained in our previous works [4,6,1]

$$I_{st}(T,t) = \frac{1}{d_0^3}\sqrt{\frac{\sigma_{eq}(T)\zeta(t)}{k_B T}}\frac{2D(T,t)}{d_0}\exp\left(-\frac{W_{c,eq}(T)\zeta(t)}{k_B T}\right), \tag{5}$$

$$D(T,t) = D_0\exp\left(-\frac{E_U\zeta(t)}{k_B T}\right), \tag{6}$$

where: k_B is the Boltzmann constant, T is the absolute temperature, T_m is melting point, d_0 is the effective size of the structural units – estimated as $d_0 = (V_M/N_A)^{1/3}$ via the crystal molar volume, V_M, and the Avogadro number, N_A, and D is the effective diffusion coefficient, with D_0 and E_U chosen to best fit the experimental crystal growth rate data assuming the (most common) screw dislocation growth model [4,6]:

$$U = D\frac{T_m - T}{8\pi d_0 T_m}\left[1 - \exp\left(-\frac{\Delta G_{\mathrm{V,eq}}\, d_0^3}{k_B T}\right)\right]. \tag{7}$$

In Eq.(5), $W_{c,eq}$ is the work of formation of a nucleus with critical size, R_c. In the case of a spherical nucleus, R_c becomes

$$R_c = 2\sigma_{eq}/\Delta G_{\mathrm{V,eq}}\,, \tag{8}$$

$$W_{c,eq} = \frac{16}{3}\pi\frac{\sigma_{\mathrm{eq}}^3}{\Delta G_{\mathrm{v,\,eq}}^2}\,, \tag{9}$$

where σ_{eq} is the surface tension of the critical nucleus/SCL interface which we estimated using Tolman's equation:

$$\sigma_{\mathrm{eq}}(T) = \frac{\sigma_0}{1+\dfrac{2\delta}{R_c(T)}}\,. \tag{10}$$

The surface tension of a planar interface, σ_0, and the Tolman parameter, δ, in Eq.(10) were used as fitting parameters to describe the experimental nucleation rates at $T > T_{max}$, which reach their steady-state values, I_{st}, during common (short) laboratory times due to the fast structural relaxation in this temperature range.

In this work, we evaluated the thermodynamic driving force for crystallization, $G_{\mathrm{V,eq}}$, through Eq.(11), derived in [14], for the case of a linear temperature dependence of the difference between the specific heat capacities of the liquid and crystal phases.

$$\Delta G_{V,eq} = \Delta H_m\left(1-\frac{T}{T_m}\right)\left(\frac{7T}{T_m+6T}\right), \tag{11}$$

where ΔH_m is the fusion enthalpy. It should be noted that Eq.(11) describes well the experimental values $\Delta G_{V,eq}$for the barium disilicate system [15].

The evolution of the structural relaxation parameter, $\zeta(t)$, can be approximated by the Kohlrausch stretched exponent law:

$$\zeta(t) = 1 + \zeta_0 \exp\left[-\left(\frac{t}{\tau_{sr}}\right)^{\beta}\right]. \tag{12}$$

The characteristic time of "nucleation" structural relaxation τ_{sr}, ζ_0, and β used as fitting parameters to achieve the best agreement between the time dependence of the number of nucleated crystals

$$N(t) = \int_0^t I_{st}(t')dt' \tag{13}$$

with experimentally measured data.

However, the analytical equations presented above (Eqs. (5) and (13)) are inadequate to analyze nucleation dynamics in the very beginning of the process, especially when a development treatment was used. The reason is that the temporal steady-state nucleation rate dependent on parameter $\zeta(t)$ (see Eq.(5)) is not reached in the early stages in a relaxing glass at $T < T_{max}$. That is why we also performed numerical simulations – based on the kinetic model of nucleation described, e.g., in [16,1] – for the initial part of the nucleation curves, with time dependent properties: diffusion coefficient, *D*, thermodynamic driving force for crystallization, $\Delta G_{\mathrm{V,eq}}$, and surface tension of the critical nucleus/SCL interface, σ.

This numerical approach is based on the calculation of a time-dependent cluster size distribution function, f_n, based on solving a set of coupled linear differential equations that describe the attachment and detachment of "structural units" to or from the clusters of the new phase:

$$\frac{df_n}{dt} = \omega_{n-}^{+}{}_{1,n} f_{n-1} + \omega_{n+}^{-}{}_{1,n} f_{n+1} - \left(\omega_{n,n}^{+}{}_{+1} + \omega_{n,n}^{-}{}_{-1}\right) f_n, \tag{14}$$

$$\omega_{n-}^{+}{}_{1,n} = K_s \frac{n^{2/3}}{d_0^2} D\zeta \begin{cases} 1 & \text{if } n \geq n^* \\ \exp\left(-\frac{W_n - W_{n-1}}{k_B T}\zeta\right) & \text{if } n < n^* \end{cases}, \tag{15}$$

$$\omega_{n+}^{-}{}_{1,n} = \omega_{n-}^{+}{}_{1,n} \exp\left(\frac{W_n - W_{n-1}}{k_B T}\zeta\right), \tag{16}$$

where: the subscript n indicates the number of "structural units" with size d_0 in the crystalline cluster; $\omega_{n,n}^{+}{}_{+1}$ is the rate at which a cluster composed of n structural units gains another unit to become an $n+1$ cluster, and $\omega_{n,n}^{-}{}_{-1}$ is the rate at which a cluster loses one unit to become a $n-1$ cluster. W_n is the work of cluster formation composed of n structural units:

$$W_n = n\Delta\mu + K_s d_0^2 \sigma n^{\frac{2}{3}}, \tag{17}$$

$$\Delta\mu = \mu_s - \mu_l = -d_0^3 \Delta G_V(T)\,. \tag{18}$$

In the case of spherical clusters, the shape factor is $K_s = (36\pi)^{1/3}$. Eqs. (14)-(16) are the basic relations from which the analytical expression for the nucleation rate (Eq.(5)) are derived.

The number density of crystals $N_n(t)$ nucleated during time t at T_n $(n > n_c(T_n))$ and N_d (t) developed at T_d $(n > n_c(T_d))$ can be estimated through the following equations:

$$N_n(t) = \sum_{n_c(T_n)}^{\infty} f(n,t), \tag{19}$$

$$N_d(t) = \sum_{n_c(T_d)}^{\infty} f(n,t), \tag{20}$$

where $n_c(T_n)$ and $n_c(T_d)$ are the critical sizes at the nucleation and development temperatures, respectively; an instant heating from T_n to T_d is assumed.

To connect the two methods of analysis of the nucleation experiments, we *corrected* (following [1]) the standard expression for the work of critical nucleus formation (Eq.(9)) *subtracting* the work, W_1, of formation a cluster consisting of a single structural unit, because such clusters are already present in the original glass. The corrected equation reads:

$$W_{c,eq} = (n_{cr} - 1)\Delta\mu + K_s d_0^2 \sigma\left(n_{cr}^{2/3} - 1\right). \tag{21}$$

4 Results

Figure 2 presents the crystal radius, R, *vs*. time plots for different temperatures. Starting from the size R_U, within the range $R_U \approx 12...20\ \mu m$, the crystal growth velocity $U = dR/dt$ increases. This interesting (novel) finding deserves a detailed analysis, and a separate work will be devoted to it. For now, to estimate the diffusion coefficient for the nucleation kinetics analysis, Eq.(6), we will use only the growth velocities, Eq.(7), for the initial range $R < R_U$, since these time intervals correspond to the nucleation times in our experiments.

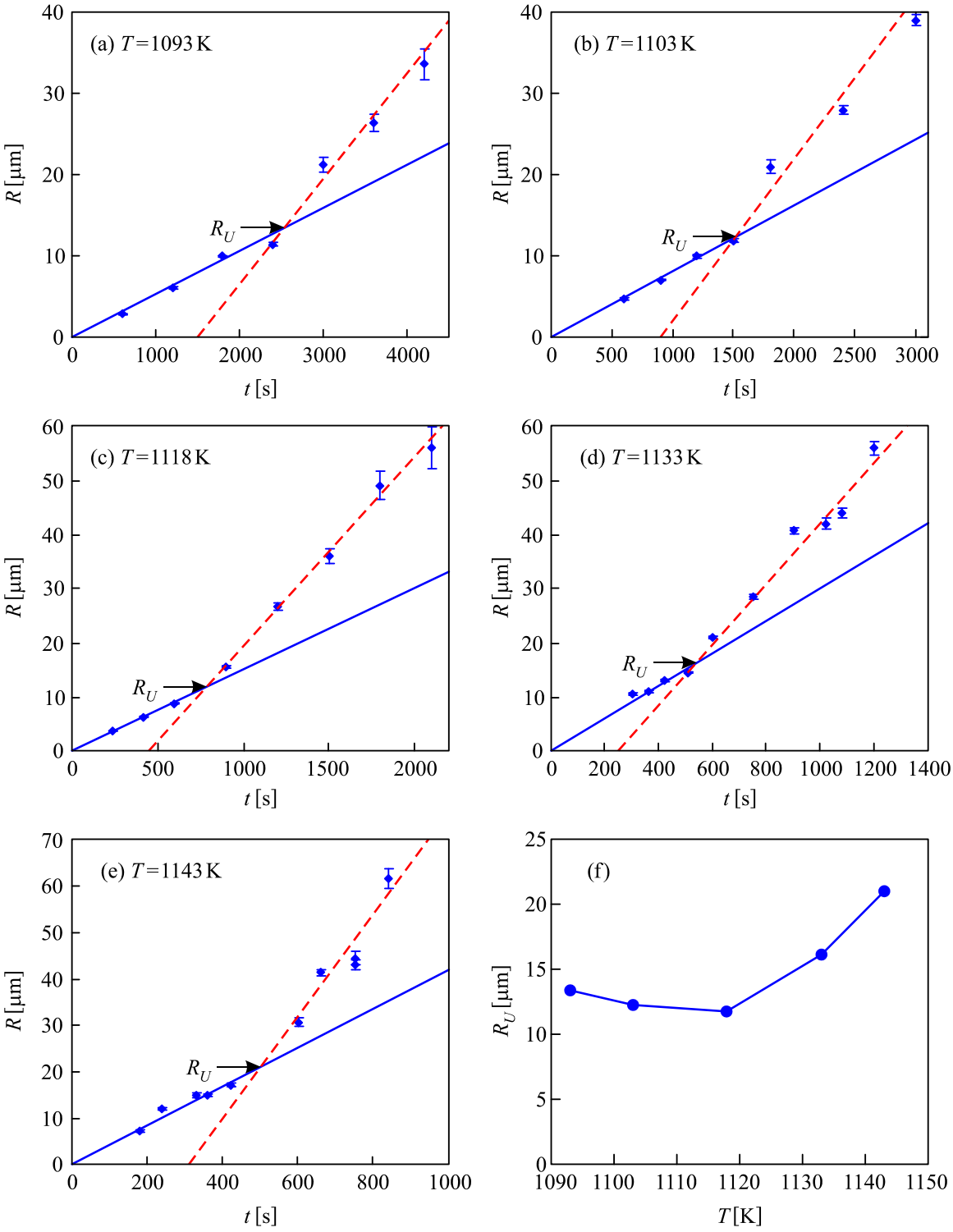

Fig. 2. (a-e) Time dependence of the crystal radius for several temperatures, and (f) R_U *vs.* temperature.

Crystal growth velocities estimated from the R *vs.* t data for $R < R_U$ for several temperatures are presented in Fig. 3. The dashed line is an Arrhenius plot describing the low temperature interval corresponding to the nucleation experiments. For comparison, it should be noted that literature data are close to ours, revealing a similar temperature dependence.

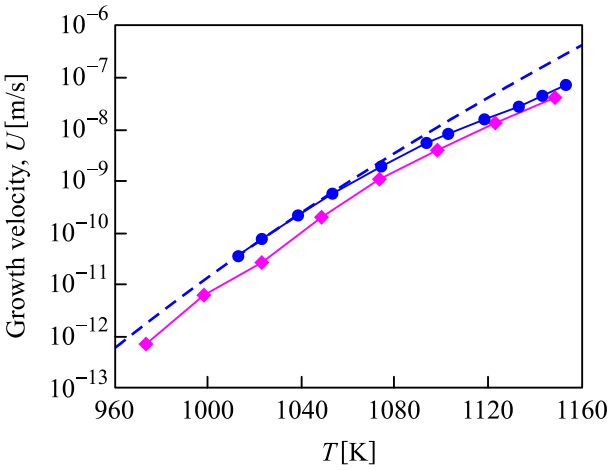

Fig. 3. Growth rate of B_5S_8 crystals in the isochemical glass as a function of temperature. Our experimental data are denoted by circles. The dashed line is the Arrhenius plot of our data at low temperatures. The rhombuses show the data of van Hoesen et al. [8].

Figure 4 shows the $N(t)$ data (the index "*d*" was omitted here for simplicity) for the lowest nucleation temperature $T = 948\text{K}$ and after development at $T_d = 1085$ K. We use this temperature to illustrate the nucleation kinetics analysis performed in the present work. Two approaches presented in Section 3 have been used for this purpose. We employed the numerical approach to describe the very beginning of the nucleation process. We considered the development stage, limited to $n_{max} = 25{,}000$ structural units in the cluster distribution function $f(n,t)$, that is, Eq.(20) for $t \le t_{max}$, where t_{max} is the time when the distribution function reaches the size n_{max}, $f(n_{max},t_{max}) = 10^8$ (that is one crystal in the laboratory sample of $10\ \text{mm}^3$). This time is shown by the vertical dashed line in the inset of Fig. 4. For $t > t_{max}$, we describe the nucleation kinetics using Eq.(13), which includes the expression for the steady-state nucleation rate:

$$N(t) = \sum_{n_{cr}(T_d)}^{n_{max}} f(n,t_{max}) + \int_{t_{max}}^{t} I_{st}(t')dt'. \qquad (22)$$

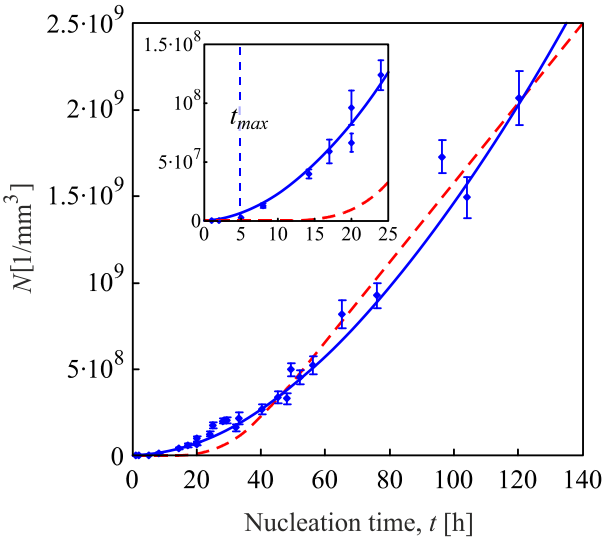

Fig. 4. Number of crystals per unit volume, $N(t)$, *vs*. nucleation time, t, at $T = 948$K. The symbols represent the experimental data, whereas the solid blue lines show fits via Eq.(20) up to $t_{max} = 5$h and Eq.(13) for $t > 5$h (details in the text). The dashed red lines were obtained via simulations based on the kinetic model of nucleation with constant D and σ, i.e., the fitting parameters that best describe the final part of the experimental $N(t)$ dependency.

Figure 5 shows the true $I(t)$ dependence estimated by the numerical simulation based on the kinetic model of nucleation considering the development stage (solid line). Is also shows the similar dependence plotted via Eq.(5) (dashed line), i.e., assuming that the nucleation rate is stationary all the time, and only changes as a result of structural relaxation.

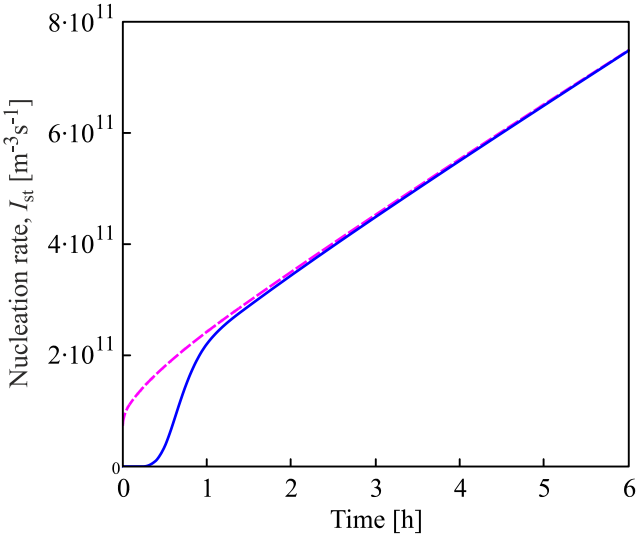

Fig. 5. Simulated $I(t)$ dependence (solid blue line) and the $I(t)$ plotted via Eq.(5) (dashed pink line) for $T = 948$K assuming a steady-state nucleation rate that changes only as a result of structural relaxation.

It can be clearly seen that the use of Eq.(5) overestimates the nucleation rate; however, starting from a certain moment, the theoretical and experimental curves practically coincide. Thus, beginning from this moment of time, t_{sw}, Eq.(5) correctly estimates the evolution of the steady-state nucleation rate (which is time dependent due to the relaxation process until it reaches the definitive state). Therefore, when describing the nucleation kinetics, we used analytical equations starting from the time t_{sw}.

The $N(t)$ computation results through Eqs. (20) and (22) are shown in Fig. 4 by the solid curve. It should be noted that both methods use the same parameter ζ (see Eq.(12)) to describe structural relaxation. As follows from Fig. 4, taking relaxation into account enables description of the experimental data over the entire range of nucleation times.

The dashed pink line in Fig. 4 shows an erroneous interpretation of the increase in $dN(t)/dt$ as the establishment of the classical stationary nucleation regime described by the CNT in the sense of Zeldovich [17,18]. This dashed pink line resulted from simulations based on the kinetic model of nucleation [1,16] with *constant D* and σ (i.e., the assumption that the crystallizing liquid remains unchanged), which served as the fitting parameters for the best description of the final part of the experimental $N(t)$ dependency. This line describes only a limited part of the $N(t)$ dependence, and is far from the experimental data for short nucleation times. This discrepancy between theory and experiment can be especially noticed in the inset plot. Thus, without considering the effect of structural relaxation, as it was done to plot the solid line, it is impossible to describe the experimental nucleation kinetics over the entire time interval.

Figure 6 shows other nucleation data and their correct description for all other temperatures studied in this work. The parameters used for plotting the solid lines are shown in Table 1. These include the parameters ζ_0, β, and τ_{sr} of the Kohlrausch relation, Eq.(12), which we used to describe the structural relaxation parameter, $\zeta(t)$, which determines the time increase of nucleation rates. Table 1 also presents the experimental nucleation rates, *I*, estimated from the final parts of the *N*(*t*) plots and the maximal value of the nucleation time-lag estimated by Eq.(23) [19], employing the minimal value of the diffusion coefficient, Eq.(6), corresponding to the very beginning of the nucleation process:

$$\tau_K = \frac{16}{3}\frac{\sigma k_B T}{D d_0^2 \Delta G_V^2}. \qquad (23)$$

Table 1. Experimental nucleation rates, I; parameters ζ_0 and β; "nucleation" structural relaxation times, τ_{sr}, obtained from fitting the experimental data to Eq. (12); classical nucleation time-lags, - τ_K, estimated through Eq. (23), for different temperatures

T [K]	I [$\mathrm{m}^{-3}\mathrm{s}^{-1}$]	ζ_0	β	τ_{sr} [s]	τ_K [s]
948	$6.3 \cdot 10^{12}$	0.05	0.45	82492	1163
958	$6.0 \cdot 10^{12}$	0.05	0.40	22115	495
968	$8.0 \cdot 10^{12}$	0.045	0.30	6330	145
978	$1.2 \cdot 10^{13}$	0.045	0.30	544	65
983	$1.0 \cdot 10^{13}$	0.045	0.28	329	43
998	$6.5 \cdot 10^{12}$	0.045	0.26	52	13
1013	$4.0 \cdot 10^{12}$	0.045	0.22	13	4.3
1023	$2.5 \cdot 10^{12}$	0.045	0.22	5.1	2.1
1038	$9.5 \cdot 10^{11}$	0.045	0.18	1.3	0.7
1053	$3.6 \cdot 10^{11}$	0.045	0.18	0.4	0.25

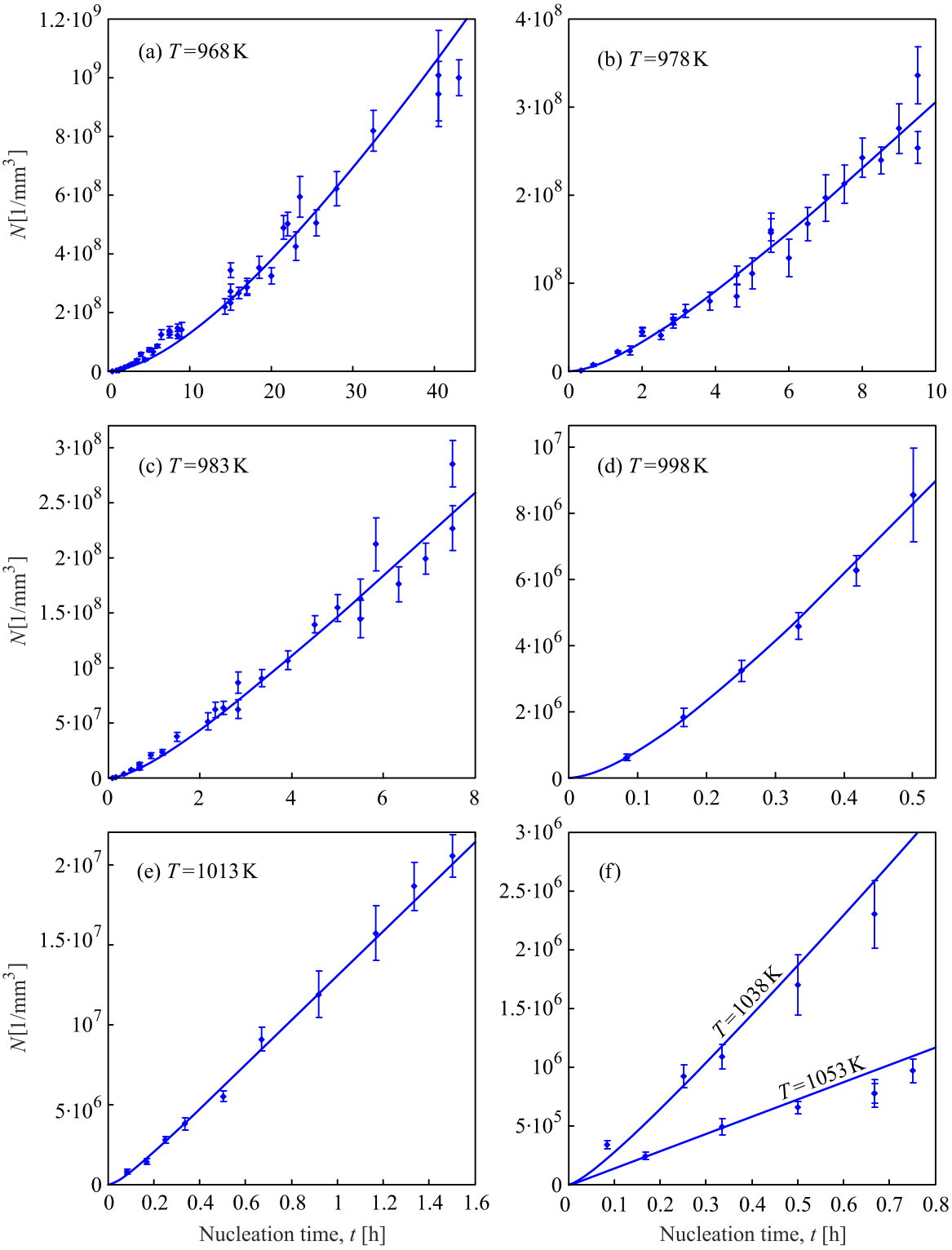

Fig. 6. Number of crystals per unit volume, $N(t)$, *vs*. nucleation time, t, for different temperatures. The symbols represent the experimental data, whereas the solid blue lines refer to the fits via Eqs. (20) and (22).

5. Discussion

As indicated in the Introduction section, one of the main tasks of this work was to expand nucleation experiments using another glass-forming system to confirm (or not) and further develop our approach for interpreting the nucleation dynamics at deep supercoolings, which were recently described in [4-6]. Often, the use of different substances allows one not only to confirm or refute previous findings, but also to discover new facts, which sometimes turn out to be the main results. This is exactly what happened in this research work after a detailed analysis of nucleation kinetics in a $5BaO{\cdot}8SiO_2$ glass. However, we will begin the next section with a discussion about the expected results, similar to those obtained earlier for glasses $Li_2O{\cdot}2SiO_2$ and $2Na_2O{\cdot}CaO{\cdot}3SiO_2$.

5.1 Structural relaxation and apparent "breakdown" of the CNT

Figure 7 shows the nucleation rate of B_5S_8 glass as a function of temperature. The circles denote the nucleation rates corresponding to the final parts of the experimental $N(t)$ plots. The dashed line shows the steady-state nucleation rate in a fully relaxed SCL calculated through Eq.(5) with $\zeta = 1$. The surface tension, $\sigma_{\mathrm{eq}}(T)$, was estimated through the Tolman's equation (Eq.(10)) with $\sigma_0 = 0.1646\ \mathrm{J/m^2}$ and $\delta = 0.0927 d_0$, which give the best description of the nucleation data for $T \geq 978\mathrm{K}$, where the nucleation experimental times were sufficient to complete structural relaxation and hence achieve the ultimate steady-state nucleation rate. T_{tmax} denotes the temperature of maximum ultimate steady-state nucleation rate. For low temperatures ($T \leq 968\mathrm{K}$), the experimental nucleation rates are less than the theoretically expected values due to incomplete structural relaxation during the (relatively short) nucleation experiments. At 948, 958 and 968 K, the nucleation rates reach 90% of the ultimate values after 487, 192 and 158 h, respectively, which significantly exceed the maximum experimental times of 120, 47 and 42 h (unfortunately, these experimental times were limited because of significant *crystal impingement*).

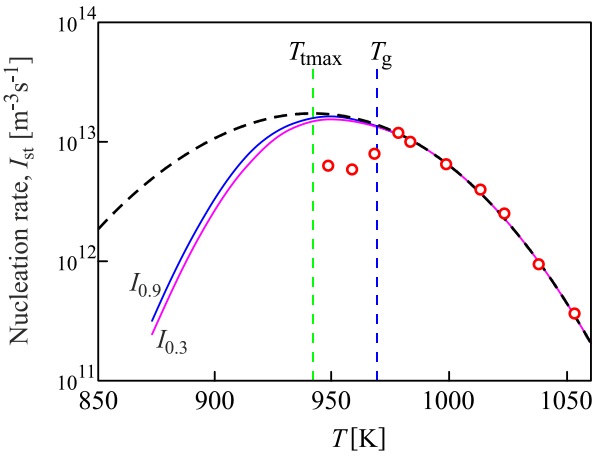

Fig. 7. Nucleation rate in B_5S_8 glass *vs*. temperature. The circles denote the experimental nucleation rates corresponding to the final parts of the experimental $N(t)$ plots. The dashed black line was calculated via Eq.(5). T_{tmax} denotes the theoretical maximum of the ultimate steady-state nucleation rate. The solid lines show the nucleation rates calculated for partly crystallized glasses with 0.3 and 0.9 crystallized volume fractions, respectively. The predicted T_{tmax} is below the experimental T_{max}.

This apparent "breakdown" of the CNT was considered recently in [**7-9**] using a glass with the same nominal composition ($5BaO{\cdot}8SiO_2$) as the glass employed here. The use of SEM allowed the authors to extremely extend the nucleation treatment time up to 115 days (~2760 h) for $T = 948$ K [**9**]. We analyzed these published data (N *vs*. t) using the methods described in Section 4. Fig. 8 shows the calculated N *vs*. t dependence and data taken from [**9**] (unfortunately, these data have a large gap between 18 and 300 h). Assuming that after $t > 1400$ h the nucleation process reaches its stationary regime (as it was done in [**9**]), we computed this part of the $N(t)$ dependence through Eq.(20) with constant values of diffusion coefficient, D, and surface tension, $\sigma_{eq,}$ used as fit parameters, neglecting structural relaxation (dashed line in Fig. 8). It can be clearly seen that this fixed set of parameters allows us to describe only the part for which the fitting was carried out, while the experimental N values for $t < 18$h are extremely far from the dashed line. Thus, we have to assume a time change of the parameters determining the nucleation rate, which is caused by the glass relaxation. We came to the same conclusion via an analysis of the nucleation kinetics of $Li_2O{\cdot}2SiO_2$ [4] and $2Na_2O{\cdot}1CaO{\cdot}3SiO_2$ [6] glasses, as well as the $5BaO{\cdot}8SiO_2$ glass focused here. Unlike the dashed line, the solid line in Fig. 9 shows fits via Eq.(20) for $t < 21$ h and Eq.(22) for $t > 21$ h with an account of the structural relaxation through Eq.(12). In this way, we can describe the nucleation experiment over the entire time interval. We also employed the experimental data from [**9**] to calculate (see details above) the $I_{st}(T)$ dependence shown in Fig. 9 by a solid line for a wide temperature interval. This figure shows that even extending the heat treatment time to 115

days at 948 K was not enough to reach the ultimate steady-state nucleation rate corresponding to the fully relaxed SCL.

It is important to note that the fitting procedure for plotting the solid line in Fig. 8 was carried out considering all experimental ($N(t)$) data available and the expected value of the steady-state nucleation rate corresponding to that temperature (see Fig. 9).

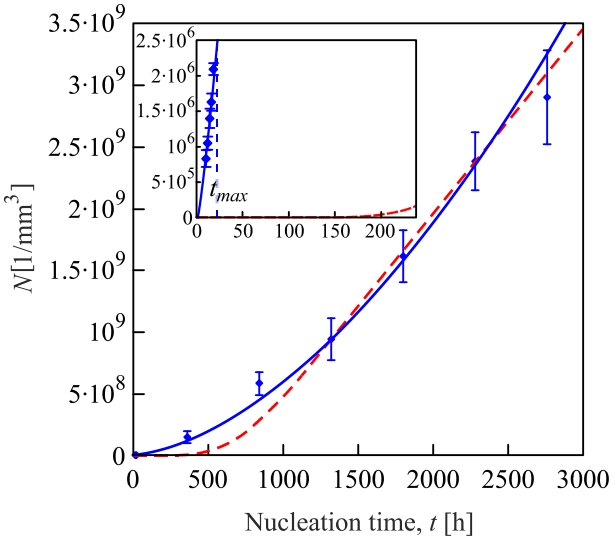

Fig. 8. Number of crystals per unit volume, $N(t)$, *vs*. nucleation time, t, at $T = 948$K for the B_5S_8 glass of ref. [**9**]. The symbols represent the experimental data of [**9**], whereas the solid blue lines show our fits via Eq.(20) up to $t_{max} = 21$ h and Eq.(22) for $t > 21$ h (details in the text). The dashed red lines were obtained here via simulations based on the cluster dynamics model with constant D and σ – the fitting parameters that best describe the final part of the experimental $N(t)$ dependence.

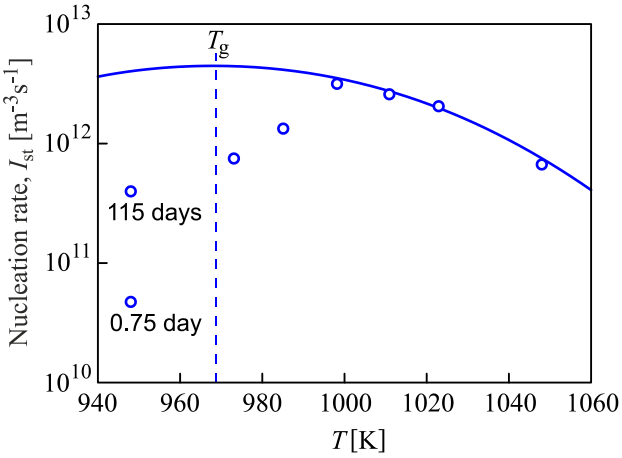

Fig. 9. Nucleation rate *vs*. temperature for the B_5S_8 glass of ref. [**9**]. Circles denote the nucleation rates corresponding to the final parts of the experimental $N(t)$ plots [**9**]. The solid line was calculated here via Eq. (5).

5.2 Structural relaxation and overall crystallization

As shown in this work and in our previous publications conducted with other two glasses [4-6], glass relaxation and its crystallization are, in general, two simultaneous processes. Relaxation and crystallization are, in principle, independent processes, but the former has a strong effect on the latter. A relevant **question** is whether at low temperatures below T_g **any glass** can completely **relax** and, accordingly**, the nucleation rate can reach the ultimate steady-state value before its complete crystallization**. To answer this question, we calculated the kinetics of overall crystallization $\alpha(t)$ via Eqs. (24-25), employing the nucleation rates, Eq.(5), and growth velocities, Eq.(7), with the same parameters $\zeta(T,t)$, characterizing the structural relaxation of glass:

$$\alpha(t) = 1 - \exp\left(- \int_0^t I(T,t')v(t-t')dt' \right), \tag{24}$$

$$v(t) = \frac{4\pi}{3}\left(\int_0^t U(t')dt' \right)^3 . \tag{25}$$

Figure 10 shows the $\alpha(t)$ for $T = 948\text{K}$. The vertical dashed lines denote the moments of time $t_{0.3}$ and $t_{0.9}$ corresponding to the 0.3 and 0.9 crystalline fractions, respectively. We calculated, via Eq.(5), the nucleation rates $I(t_{0.3})$ and $I(t_{0.9})$ for several temperatures. The results are shown in Fig. 7 by solid lines. For B_5S_8 glass, at temperatures below T_{tmax}, the *residual SCL disappears* before it reaches the equilibrium state and, accordingly, the nucleation rates will never reach their ultimate steady-state values.

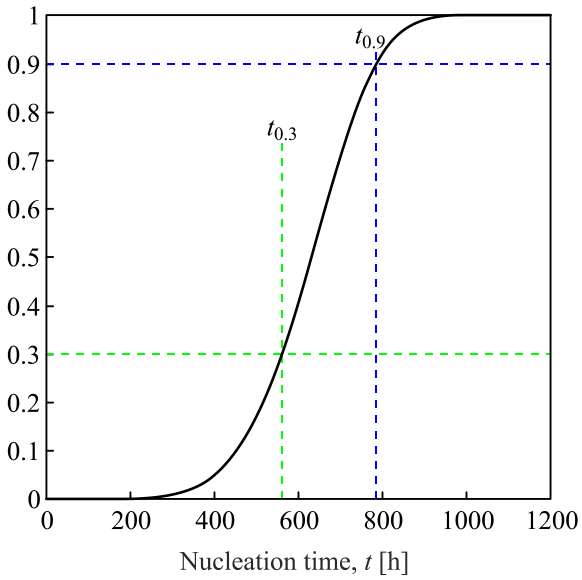

Fig. 10. Crystalline volume fraction *vs*. nucleation time at $T = 948\text{K}$. The vertical dashed lines denote the moments of time $t_{0.3}$ and $t_{0.9}$ corresponding to the 0.3 and 0.9 crystalline fractions, respectively.

5.3 Structural relaxation times of the SCL and glass

The traditional approach to the glass transition problem is developed in the kinetic theory of glass transition (KTGT) (see, e.g., [20]). The cooling or heating rates are the key parameters of the KTGT. Using the results of isothermal nucleation experiments, we estimated the structural relaxation times, τ_{sr}, as a function of temperature (Table 1). This dependence, shown in Fig. 11, revealed a step-like behavior of τ_{sr}: in a relatively narrow temperature interval $T_g^* - 8K < T < T_g^* + 8K$, τ_{sr} increases with decreasing temperature by a factor 4, resulting in longer relaxation time, $\tau_{glass}(T)$, in a glass state as compared to $\tau_{liq}(T)$ in the SCL.

The structural relaxation time, $\tau_{sr}(T)$, can be fitted by the dependence

$$\tau_{sr}(T) = \tau_{glass}(T)\kappa\left(T_g^* - T\right) + \tau_{liq}(T)\kappa\left(T - T_g^*\right), \tag{26}$$

where $\kappa(T) = 0.5\left(\tanh\left(T/\Delta T\right) + 1\right)$, and the glass and liquid relaxation times are given by the VFT equation,

$$\tau_{glass}(T) = \tau_{0,glass}\exp\left(\frac{E_0}{k_B(T - T_0)}\right), \tag{27}$$

$$\tau_{liq}(T) = \tau_{0,liq}\exp\left(\frac{E_0}{k_B(T - T_0)}\right). \tag{28}$$

Here: $\tau_{0,liq} = 3.92 \cdot 10^{-13} s$, $\tau_{0,glass} = 4\tau_{0,liq} = 1.57 \cdot 10^{-12} s$, $E_0 = 2.229 \cdot 10^{-19} J$, $T_g^* = T_g + 4\text{K} = 973\text{K}$, and $T_0 = 602.3\text{K}$.

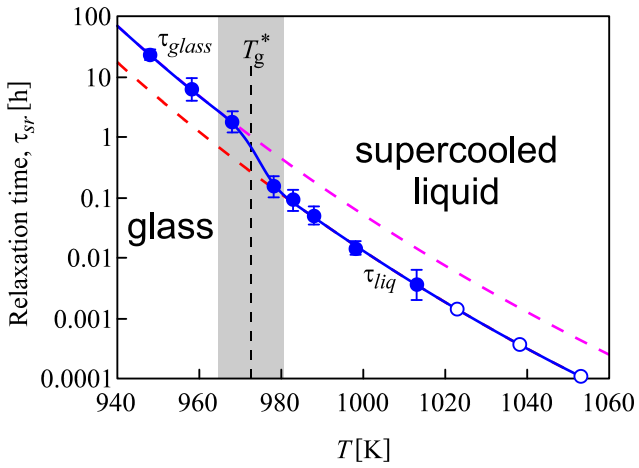

Fig. 11. Relaxation time as a function of temperature. The gray band shows a transition temperature interval, $T_g^* - 8K < T < T_g^* + 8\ K$, between $\tau_{sr} = \tau_{glass}$ and $\tau_{sr} = \tau_{liq}$. The full and empty circles indicate the relaxation times calculated from nucleation data (see Eq. (12)) and extrapolated to high temperatures, respectively.

It should be noted that this interval is close to the glass transition interval estimated via the DSC at moderate heating rates, $T_g^* \approx T_g$. Special attention should be paid to the fact that the interval in which fast change in the relaxation time occurs corresponds to quite definite temperatures, while the glass transition interval depends on the heating or cooling rates of the sample.

It can be assumed that the right side of the dependence $\tau_{sr}(T)$, $T > T_g^* + 8\ K$, refers to the SCL, while the left side, $T < T_g^* - 8K$, refers to the glassy state.

Note that the activation energies of structural relaxation of the glass and SCL do not differ within the error limits. Consequently, the longer relaxation time of the glassy state is due to the larger pre-exponential term. Both states are metastable with respect to the crystalline state, and change monotonically with temperature. This finding requires further detailed analysis, both from theoretical and experimental points of view.

6 Conclusions

We performed a combination of detailed experiments and theoretical analysis (analytical and numerical) for a B_5S_8 glass heated somewhat above and below T_g which revealed that:

i) The so-called "breakdown" of the CNT, often reported for temperatures below T_g, is just an artefact because the experimental nucleation times are often not long enough to complete structural relaxation and hence reach the ultimate steady-state nucleation rate. This finding corroborates our recent results for two other glasses (LS2 and 213).

ii) The predicted T_{tmax} is lower than the "experimental" T_{max}, as found for LS2 and 213 glasses.

iii) For the first time, we found an inflection in the temperature dependence of the structural relaxation times (inferred from nucleation experiments) in the glass transition region: the characteristic relaxation times for the SCL are 4 times shorter than those for the glassy state.

iv) Finally, also for the first time, the current results and analyses show that, for $5BaO{\cdot}8SiO_2$ glass – and likely for other glasses that display very high nucleation and growth rates – complete structural relaxation and the ultimate steady-state nucleation regime cannot be reached at some temperatures below T_{max} because of the premature crystallization of the samples. This new finding further explains the failure of several previous works to reach the definitive steady-state nucleation regime at low temperatures, which lead to the erroneous notion of a "breakdown" of the CNT below $\sim T_g$.

These combined results shed light on crucial dynamic aspects of deeply supercooled liquids and glasses.

Acknowledgements

We are grateful to Coordenação de Aperfeiçoamento de Pessoal de Nível Superior - (CAPES) Brazil, grant no. 88887.468838/2019-00, National Council for Scientific and Technological Development (CNPq), grant number 141816/2018-0 (LRR), and São Paulo Research Foundation (FAPESP), Cepid Project no. 2013/007793-6 for the funding received. This study was financed in part by the Coordenação de Aperfeiçoamento de Pessoal de Nível Superior – Brasil (CAPES) – Finance Code 001.

References

[1] A.S. Abyzov, J.W.P. Schmelzer, V.M. Fokin, E.D. Zanotto, Crystallization of Supercooled Liquids: Self-Consistency Correction of the Steady-State Nucleation Rate, Entropy. 22 (2020) 1–28. https://doi.org/10.3390/e22050558

[2] L. Gránásy, P.F. James, Transient nucleation in oxide glasses: The effect of interface dynamics and subcritical cluster population, J. Chem. Phys. 111 (1999) 737 – 749. https://doi.org/10.1063/1.479353.

[3] L. Gránásy, P.F. James, Nucleation in Oxide Glasses: Comparison of Theory and Experiment, Proc. R. Soc. A Math. Phys. Eng. Sci. 454 (1998) 1745–1766. https://doi.org/10.1098/rspa.1998.0230.

[4] V.M. Fokin, A.S. Abyzov, N.S. Yuritsyn, J.W.P. Schmelzer, E.D. Zanotto, Effect of structural relaxation on crystal nucleation in glasses, Acta Mater. 203 (2021) 9–11. https://doi.org/10.1016/j.actamat.2020.11.014.

[5] J.W.P. Schmelzer, T. V. Tropin, V.M. Fokin, A.S. Abyzov, E.D. Zanotto, Effects of glass transition and structural relaxation on crystal nucleation: Theoretical description and model analysis, Entropy. 22 (2020) 1–36. https://doi.org/10.3390/e22101098.

[6] L.R. Rodrigues, A.S. Abyzov, V.M. Fokin, E.D. Zanotto, Effect of structural relaxation on crystal nucleation in a soda-lime-silica glass, J. Am. Ceram. Soc. 104 (2021) 3212–3223. https://doi.org/10.1111/jace.17765.

[7] X. Xia, D.C. van Hoesen, M.E. Mckenzie, R.E. Youngman, O. Gulbiten, K.F. Kelton, Time-dependent nucleation rate measurements in $BaO{\cdot}2SiO_2$ and $5BaO{\cdot}8SiO_2$ glasses, J. Non. Cryst. Solids. 525 (2019) 119575. https://doi.org/10.1016/j.jnoncrysol.2019.119575.

[8] D.C. van Hoesen, X. Xia, M.E. Mckenzie, K.F. Kelton, Crystallization kinetics in a $5BaO{\cdot}8SiO_2$ glass, J. Non. Cryst. Solids. 553 (2021) 120479.

[9] X. Xia, D.C. Van Hoesen, M.E. Mckenzie, R.E. Youngman, K.F. Kelton, Low-temperature nucleation anomaly in silicate glasses shown to be artifact in a $5BaO{\cdot}8SiO_2$ glass, Nat. Commun. 12:2026 (2021) 1–6. https://doi.org/10.1038/s41467-021-22161-9.

[10] M.E. McKenzie, B. Deng, D.C. van Hoesen, X. Xia, D.E. Baker, A. Rezikyan, R.E. Youngman, K.F. Kelton, Nucleation pathways in barium silicate glasses, Sci. Rep. 11:69 (2021) 1–15. https://doi.org/10.1038/s41598-020-79749-2.

[11] M.H.R. Acosta, L.R. Rodrigues, E.D.G. Castro, E.D. Zanotto, Assessing glass-ceramic homogeneity and nucleation self-correlation by crystallization statistics, J. Am. Ceram. Soc. 104 (2021) 4459–4470. https://doi.org/10.1111/jace.17815.

[12] V.M. Fokin, E.D. Zanotto, N.S. Yuritsyn, J.W.P. Schmelzer, Homogeneous crystal nucleation in silicate glasses: A 40 years perspective, J. Non. Cryst. Solids. 352 (2006) 2681–2714. https://doi.org/10.1016/j.jnoncrysol.2006.02.074.

[13] E.D. Zanotto, P.F. James, A theoretical and experimental assessment of systematic errors in nucleation experiments, J. Non. Cryst. Solids. 124 (1990) 86–90. https://doi.org/10.1016/0022-3093(90)91084-5.

[14] H.B. Singh, A. Holz, Stability limit of supercooled liquids, Solid State Commun. 45 (1983) 985–988. https://doi.org/10.1016/0038-1098(83)90973-0.

[15] A.S. Abyzov, V.M. Fokin, A. Mendes, E.D. Zanotto, J.W.P. Schmelzer, The effect of elastic stresses on the thermodynamic barrier for crystal nucleation, J. Non. Cryst. Solids. 432 (2016) 325–333. https://doi.org/10.1016/j.jnoncrysol.2015.10.029.

[16] K.F. Kelton, A.L. Greer, Nucleation in condensed matter: applications in materials and biology, Elsevier, Oxford, 2010.

[17] Y.I. Frenkel, The Kinetic Theory of Liquids, Oxford University Press, Oxford, 1946.

[18] K.F. Kelton, A.L. Greer, C. V. Thompson, Transient nucleation in condensed systems, J. Chem. Phys. 79 (1983) 6261 – 6276. https://doi.org/10.1063/1.445731.

[19] D. Kashchiev, Solution of the non-steady state problem in nucleation kinetics, Surf. Sci. 14 (1969) 209–220.

[20] J.W.P. Schmelzer, I.S. Gutzow, Glasses and the Glass Transition, WILEY-VCH Verlag GmbH & Co.KGaA, 2011.